J. Marine Sci. Appl. (2017) 16: 465-472
DOI: https://doi.org/10.1007/s11804-017-1439-1

A Numerical Study on Piezoelectric Energy Harvesting by Combining Transverse Galloping and Parametric Instability Phenomena

Guilherme Rosa Franzini*, Rebeca Caramêz Saraiva Santos and Celso Pupo Pesce

Escola Politécnica, University of São Paulo, São Paulo SP 05508-030, Brazil

Abstract: This paper aims to numerically investigate the effects of parametric instability on piezoelectric energy harvesting from the transverse galloping of a square prism. A two degrees-of-freedom reduced-order model for this problem is proposed and numerically integrated. A usual quasi-steady galloping model is applied, where the transverse force coefficient is adopted as a cubic polynomial function with respect to the angle of attack. Time-histories of nondimensional prism displacement, electric voltage and power dissipated at both the dashpot and the electrical resistance are obtained as functions of the reduced velocity. Both, oscillation amplitude and electric voltage, increased with the reduced velocity for all parametric excitation conditions tested. For low values of reduced velocity, 2:1 parametric excitation enhances the electric voltage. On the other hand, for higher reduced velocities, a 1:1 parametric excitation (i.e., the same as the natural frequency) enhances both oscillation amplitude and electric voltage. It has been also found that, depending on the parametric excitation frequency, the harvested electrical power can be amplified in 70% when compared to the case under no parametric excitation.
Keywords: transverse galloping, energy harvesting, piezoelectricity, parametric instability, numerical simulations

Article ID: 1671-9433(2017)04-0465-08

1 Introduction

Fluid-structure interaction phenomena usually involve self-excited oscillations. Such Flow-Induced Vibrations (FIV) can be either resonant (such as, for example, vortex-induced vibrations - VIV) or non-resonant (flutter and galloping). A very common approach is to focus on FIV mitigation. However, there is another class of investigations that aims to collect part of the kinetic energy from the structure, converting it into another class of energy, such as potential or electrical energy. It is important to emphasize that most of the investigations on the electromechanical energy conversion from FIV focuses on low-power devices.

Consider firstly energy harvesting from VIV. One of the pioneer devices is Vortex-Induced Vibrations Aquatic Clean Energy (VIVACE). Details concerning this device can be found in Bernitsas *et al*. (2006a; 2006b). For another kind of vibrating systems, cables, numerical studies described in Grouthier *et al.* (2012, 2014) focused on the influence of the structural damping parameter and the ratio between the structural natural frequency and the vortex shedding frequency. Additionally, the authors investigated the effects of distributed energy harvesters on flexible cylinders.

Energy harvesting from flutter and galloping were investigated from experimental point-of-view (see, *e.g.*, Fernandes and Armandei (2014)) or through numerical simulations (Barrero-Gil *et al*. (2010) and Bibo and Daqaq (2013)). Regarding energy conversion mechanisms, electromagnetic effects (see Tang *et al.* (2009)) or piezoelectricity (Doaré and Michelin (2011), Mehmooh *et al.* (2013) and Xia and Michelin (2015)) are usually found in the literature.

Another class of interesting dynamic problems is the parametric excitation, which may occur if one or more parameters of the equation of motion depend explicitly on time. A particular category of parametric excitation problem is composed by systems in which the stiffness depends harmonically on time, leading to the Mathieu's equation. Depending on the values of frequency and amplitude of the stiffness variation, the trivial solution may become unstable, giving rise to oscillatory response. A common tool to check the stability of the undamped Mathieu's equation is the Strutt's diagram. The textbooks written by Nayfeh and Mook (1979) and Meirovitch (2003) provide excellent didactic material on such a theme.

Parametric excitation may occur in slender offshore structures such as tethers used in Tension Leg Platforms (TLPs) and risers. Further information regarding different arrangements commonly found in the offshore engineering scenario can be found in Faltinsen (1993). In the slender offshore structures aforementioned, the geometric stiffness is dominant. The motions of the floating units cause tension modulation and, hence, modulation on its geometric stiffness. Depending on the amplitude and, mainly, the frequency of the tension modulation, lateral motions may then be observed.

Examples of studies on parametric instability in risers and

Received date: 07-Dec-2016
Accepted date: 14-Oct-2017
Foundation item: Supported by National Research Council – CNPq for Grants 310595/2015-0 and 308990/2014-5
***Corresponding author Email:** gfranzini@usp.br

© Harbin Engineering University and Springer-Verlag GmbH Germany 2017

TLP's tethers can be found in Patel and Park (1991), Simos and Pesce (1997), Franzini *et al.* (2015) and Franzini and Mazzilli (2016). Furthermore, the paper written by Franzini *et al*. (2016a) investigates the combined effects of parametric excitation and vortex-induced vibration, showing an enhancement of oscillation amplitudes.

In this brief literature overview, energy harvesting from FIV as well as some aspects of oscillations induced by parametric excitation, particularly in the offshore engineering scenario, were mentioned. However, at least to the authors' knowledge, there is a lack of investigations regarding the effects of parametric instability on piezoelectric energy harvesting from from FIV.

It is important to highlight that the parametric excitation may be imposed through an active system, or naturally, driven by environmental conditions. An example of this second case is the case of Mathieu's instability of risers and tethers, caused by the wave induced motion of the floating platform. Another possible source of parametric excitation may be provided by an external electro-mechanical system. Such closed-loop system must be designed such as to impose forces proportional to the displacements, emulating the effect of a time-dependent spring stiffness. Notice, however, that the energy harvesting efficiency of this latter system would have to take the energy provided to the electromechanical system into account.

The objective of this paper is to numerically investigate the influence of parametric excitation on piezoelectric energy harvesting from the transverse galloping of a square prism. Oscillation amplitudes, electric voltage harvested, power dissipated at the electrical resistance and at the dashpot are investigated at two excitation frequency ratios with respect to the natural frequency of the system,. This work gives continuity to the analysis described in Franzini *et al*. (2016b), but considering a nondimensional set of differential equations for the electro-fluid-mechanic system, exploring new numerical examples and enhancing discussions. Furthermore, the range of reduced velocity hereing presented is enlarged when compared to the previous contribution. New findings are obtained for large reduced velocities. Finally, it is important to emphasize that this paper does not present any consideration regarding the power necessary to externally trigger Mathieu's instability, despite the practical importance such a study might have.

The following sections present the mathematical model and discussion on some results. Finally, final remarks are presented.

2 Mathematical model

The problem herein investigated concerns a rigid square prism of length L, cross-section dimension D and structural mass m_s. The prism is assembled to an elastic support with linear damping of constant c and time-dependent stiffness $k(t)$. The free-stream velocity is U_∞. The piezoelectric patch is modeled by means of equivalent capacitance, electric resistance and electromechanical coupling terms C_p, R and θ respectively. Fig. 1 sketches the problem herein investigated.

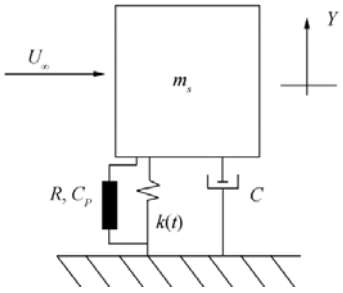

Fig. 1 Schematic representation of the problem

Following Franzini *et al.* (2016b), a model combining transverse galloping, parametric excitation and the piezoelectric phenomenon, is adopted as given in Eqs. (1) and (2).

$$\left(m_s+m_a\right)\ddot{Y}+c\dot{Y}+\frac{1}{2}\rho C_D DL\dot{Y}\left|\dot{Y}\right|+ k\left(t\right)Y-\theta V=\frac{1}{2}\rho U_\infty^2 DLC_y \tag{1}$$

$$C_P\dot{V}+\frac{V}{R}+\theta\dot{V}=0 \tag{2}$$

In Eq. (1), notice that two models have been simply combined: the equation of motion for pure parametric excitation (see, for example, Patel and Park (1991) and that from pure galloping (Païdoussis *et al.* (2011). This equation is excited by the dynamics of the piezoelectric system, which follows the constitutive Eq. (2), adopted in Mehmood *et al*. (2013).

As a fact, the used galloping model is well known in the literature. Likewise, Mathieu's type parametric excitation is a phenomenon studied extensively. Indeed, an experimental investigation focusing on the concomitant effects of galloping and parametric excitation is not a trivial task. If done, would serve as a paradigmatic result for the model validity. This, however, has been left as a recommended further work. The purpose of the present paper, at this very moment, is, relying on the validity of such combination hypothesis, to assess the sensitivity of the system response with respect to the variation of some of the controlling parameters.

Introducing the parameters $\omega_n=\sqrt{\frac{\bar{k}}{m_a+m_s}}$, $\Delta=\sqrt{\frac{\Delta k}{m_a+m_S}}$, $2\omega_n\zeta_s=\frac{c}{m_S+m_a}$, Eqs. (1) and (2) are rewritten as:

$$\ddot{Y}+\frac{c}{\left(m_s+m_a\right)}\dot{Y}+\frac{\rho C_D DL\dot{Y}\left|\dot{Y}\right|}{2\left(m_s+m_a\right)}+\left(\omega_n^2+\Delta^2\cos\left(\Omega t\right)\right)Y- \frac{\theta}{\left(m_s+m_a\right)}V=\frac{\rho U_\infty^2 DLC_y}{2\left(m_s+m_a\right)} \tag{3}$$

$$C_P\dot{V}+\frac{V}{R}+\theta\dot{Y}=0 \tag{4}$$

A set of nondimensional quantities may then be defined as:

$$y=\frac{Y}{D},\tau=t\omega_n,m^*=\frac{m_s}{\rho D^2 L},U_r=\frac{U_\infty}{\omega_n D},$$

$$\sigma_1=\frac{\theta^2}{\left(m_a+m_s\right)C_P\omega_n^2},\sigma_2=\frac{1}{RC_P\omega_n},$$

$$v=\frac{V}{V_0}=\frac{V\theta}{\left(m_a+m_s\right)\omega_n^2 D}$$

Beyond this point, $\dot{y}$ indicates the derivative of the nondimensional variable y with respect to the nondimensional time τ. The mathematical model can then be rewritten in the nondimensional form as:

$$\ddot{y}+a_1\dot{y}+\left(1+\delta\cos\left(n\tau\right)\right)y+a_2\left|\dot{y}\right|\dot{y}-v=a_3C_y \tag{5}$$

$$\dot{v}+\sigma_2 v+\sigma_1\dot{y}=0 \tag{6}$$

being:

$$\delta=\frac{\Delta k}{\bar{k}}=\left(\frac{\Delta}{\omega_n}\right)^2,\ n=\frac{\Omega}{\omega_n}a_1=2\zeta_s,$$

$$a_2=\frac{C_D}{2\left(m^*+C_a\right)},\ a_3=\frac{U_r^2}{2\left(m^*+C_a\right)}$$

Notice that δ and n represent, respectively, the amplitude and the frequency of the parametric excitation in the nondimensional form. U_r is usually named as reduced velocity.

Herein, the cross-wise coefficient will be evaluated by using the *quasi*-steady hypothesis, together with a third-order polynomial approximation:

$$C_y=\sum_{k=1}^{3}A_k\left(\frac{\dot{Y}}{U_\infty}\right)^k=\sum_{k=1}^{3}A_k\left(\frac{\dot{y}}{U_r}\right)^k \tag{7}$$

According Blevins (2001), the quasi-steady hypothesis is valid if:

$$U_r=\frac{U_\infty}{\omega_n D}>\frac{20}{2\pi}=3.19 \tag{8}$$

Besides oscillations and electric voltage, we also investigate the harvested power from the electro-fluid-mechanical system; particularly, the power dissipated at the dashpot (P_D) and the electrical power available in the piezoelectric material (P_{el}). These quantities are also made nondimensional, as follows:

$$\eta_1=\frac{|P_D|}{1/2\rho U_\infty^3 DL}=\frac{4\zeta_s}{U_r^3}\left(C_a+m^*\right)\dot{y}^2 \tag{9}$$

$$\eta_2=\frac{P_{el}}{1/2\rho U_\infty^3 DL}=\frac{2}{U_r^3}\frac{\sigma_1}{\sigma_2}\left(C_a+m^*\right)v^2 \tag{10}$$

Notice that the term $1/2\rho U_\infty^3 DL$ is the flux of fluid kinetic energy across a surface with area equal to the frontal area of the prism. Hence, the quantities η_1 and η_2 may be interpreted as energy harvesting efficiency parameters.

Finally, it is interesting to compute the increase of energy harvesting efficiency caused by parametric excitation. In this sense and following Franzini *et al*. (2016b), the following parameters are introduced:

$$\gamma_1(n)=\frac{\overline{\eta}_1(n)}{\eta_1^0} \tag{11}$$

$$\gamma_2(n)=\frac{\overline{\eta}_2(n)}{\eta_2^0} \tag{12}$$

where the bar indicates time-averaging (considering only steady-state response) and the superscript 0 refers to the case under no parametric excitation.

3 Simulations, results and discussion

The system of equations that governs the electro-fluid-mechanic system in its nondimensional form (Eqs. (5) and (6)) were numerically integrated using a 4th–5th order Runge-Kutta scheme, using MATLAB® ode45 function. The simulations were carried out with a time-step $\Delta\tau$=0.01 up to the maximum nondimensional time $\tau_{\max}=500$. Responses were considered in the interval $\tau>400$ guaranteeing a steady state regime.

Herein, focus is put on the range $5<U_r<30$, extending the range previously investigated in Franzini *et al*. (2016b), which considered reduced velocities up to 10.

Table 1 presents the parameters kept invariant along the simulations. Some comments must be made. It is well known that both C_a and C_D are strongly dependent on the flow characteristics, and hence on the prism oscillations, what gives rise to another source of nonlinearities. The proper consideration of the dependence of these coefficients on the oscillation amplitude is, in fact, a nontrivial task, which is left for a further work.

The value of added mass coefficient C_a was taken based on potential flow theory (see Korotkin (2009)). The drag coefficient C_D was assumed to be equal to that obtained from experiments with fixed bodies. It was adopted C_D=2.05, from Hoerner (1965).

Table 1 Simulations parameters

Parameter	Value
m^*	5
C_a	1.5
ζ_s	0.01
C_D	2.2
σ_1	0.015 4
σ_2	0.2653
A_1	2.69
A_2	0
A_3	−168.4

For the piezoelectric system model, the nondimensional parameters were obtained by considering the same values of θ, C_p and R used by Mehmood *et al.* (2013), previously adopted in Franzini *et al.* (2016b). The coefficients A_1, A_2 and A_3 were obtained from a third-order polynomial fit for the cross-wise force coefficient C_y Further details regarding this polynomial fit can be found in Païdoussis *et al.* (2011).

Firstly, we consider two cases: (i) no parametric excitation and (ii) parametric excitation with $\delta = 0.5$ and two frequencies-ratio values, n, namely n=1 and n=2.

Figs. 2 and 3 present, respectively, the standard-deviations of nondimensional displacement and electric voltage as functions of reduced velocity U_r. The mentioned plots clearly reveal a monotonic and upward trend of these quantities with U_r in case (i).

Qualitative and quantitative differences are observed when parametric excitation occurs. Case (ii) at n=1 shows an enhancement of both the structural oscillations and the electric voltage at the load resistance, for practically the whole range of reduced velocities simulated. On the other hand, at n=2 the standard-deviations of both $y(\tau)$ and $v(\tau)$ are larger than those obtained under no parametric excitation, in the range $20<U_r<25$.

A jump can be noticed in both $y(\tau)$ and $v(\tau)$ plots at $U_r \approx 20$, for the case n=2. A large increasing rate with U_r may be observed as well, for n=1, at $U_r \approx 14$. In fact, such a sudden amplitude increase is an interesting finding, concerning energy harvesting, not observed in the absence of parametric excitation.

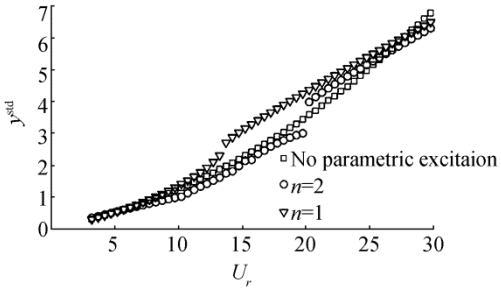

Fig. 2 Standard-deviation of $y(\tau)$ as functions of reduced velocity

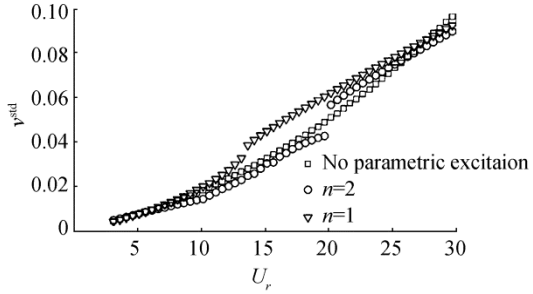

Fig. 3 Standard-deviation of $v(\tau)$ as functions of reduced velocity

Aiming at discussing the response jump at n=2, Figs. 4 and 5 are plotted, showing the time-history $y(\tau)$ and the corresponding amplitude spectrum at two reduced velocities, namely U_r=19.7 and 20.2 Such a jump is accompanied by a decrease in $\hat{f}_d = \omega_d / \omega_n$, being ω_d the dominant oscillation frequency. Note that the spectral distribution at U_r=20.2 is narrower than that at U_r=19.7, with less subharmonics.

The variation of the dominant frequency is important not only as an interesting aspect regarding the structural dynamics but also regarding the power dissipated at the dashpot. As shown in Eq. (9), the power dissipated at the dashpot depends on the velocity squared and, consequently, on the square of the nondimensional oscillation frequency.

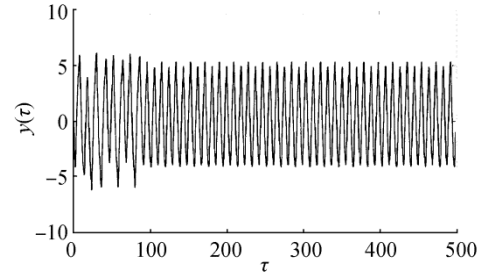

(a) $y(\tau)$

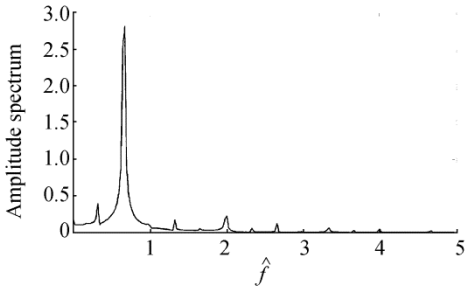

(b) Amplitude spectrum

Fig. 4 Time-history $y(\tau)$ and respective amplitude spectrum; n=2, U_r=19.7

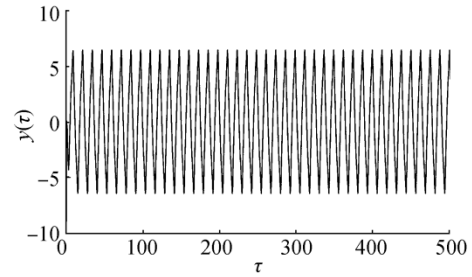

(a) $y(\tau)$

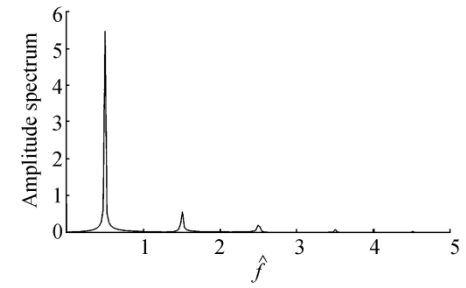

(b) Amplitude spectrum

Fig. 5 Time-history $y(\tau)$ and respective amplitude spectrum; n=2, U_r=20.2

Fig. 6 presents the variation of the nondimensional dominant oscillation frequency as functions of U_r. Notice that in the no parametric excitation case, the dominant frequency decreases with U_r. Considering now the parametric excitation case n=1, a decrease in the values of

$\hat{f}_d$ is observed in the range 3.2<U_r<14. In the range U_r>14, a constant value $\hat{f}_d$ is obtained.

On the other hand, the case n=2 reveals distinct response regimes. For U_r<11, the dominant frequency matches the natural frequency of the prism under pure parametric excitation. In fact, this is not surprising, since systems under combined parametric excitation and hydrodynamic drag force exhibits steady-state response with frequency equal to the corresponding natural frequency, if the stiffness is taken as its averaged value $\bar{k}$.

Hence, for this range of reduced velocities, parametric instability dominates the response when compared to galloping phenomena. After a monotonic decreasing trend, the dominant frequency reaches $\hat{f}_d = 0.7$ in the range 16<U_r<20. Finally, for U_r>20, the dominant oscillation frequency is constant and equal to 0.5.

This puzzling behavior regarding the dominant oscillation frequency is certainly an interesting but non-trivial aspect to be explained. Perturbation methods such as, for example, the method of multiple scales, might be used to obtain new insights.

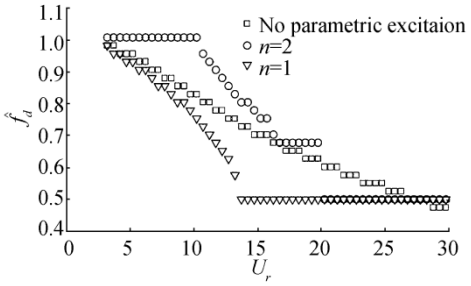

Fig 6 Nondimensional dominant oscillation frequency as function of reduced velocity

Attention is now directed to the harvested power at the dashpot and at the electrical resistance. As already mentioned, these quantities were made nondimensional and the quantities η_1 and η_2 represent the energy harvesting efficiency. It is interesting to point out that some investigations (see, for example, Grouthier *et al*. (2012, 2014) and Xia and Michelin (2015)) discuss energy harvesting just considering the power dissipated at the dashpot without mentioning how to convert it into another form such as, for example, electrical power. In fact, the power dissipated at the dashpot can be converted, for example, in heat. Obviously, the efficiency of this conversion must be taken into account in the design of a particular device for energy harvesting from flow-induced vibrations.

Figs. 7 and 8 present, respectively, the time-averaged nondimensional powers $\bar{\eta}_1$ and $\bar{\eta}_2$ (see Eqs. (9) and (10)) as functions of reduced velocity. Firstly, we analyze the variation of the power dissipated at the dashpot $\bar{\eta}_1$. As can be seen in Fig. 7, there is no significant difference between the no parametric excitation case and those with parametric excitation at n=1 and n=2. For all conditions simulated, $\bar{\eta}_1$ presents a monotonic and practically linear upward trend with U_r.

As can be seen in Fig. 8, the variations of $\bar{\eta}_2$ with U_r are more complex and depend on the parametric excitation frequency. Considering firstly the case with no parametric excitation, $\bar{\eta}_2$ decreases with the reduced velocity up to U_r>15. Beyond this value, a practically constant value is reached. The condition with n=1 indicates an enhancing of the attained time-averaged electrical power harvested for practically the whole range of reduced velocities simulated. Notice also the presence of a local maximum at $U_r \approx 14$. In fact, it is not surprising this local maximum since an increase in the standard-deviation of electric voltage was observed (see Fig. 3).

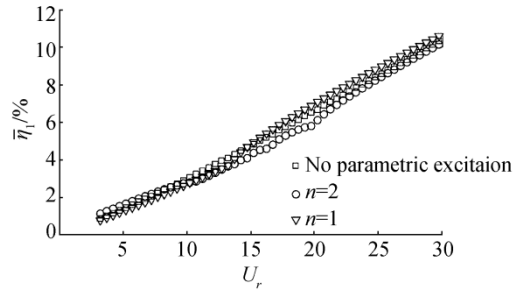

Fig. 7 Time-averaged nondimensional harvested power at the dashpot, η_1, as functions of reduced velocity

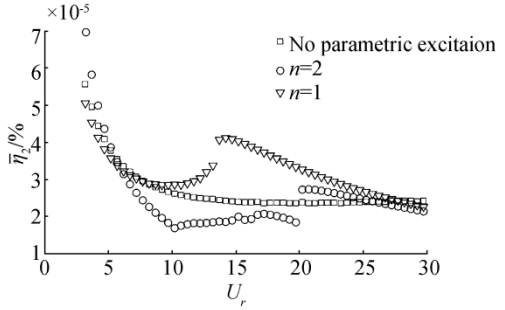

Fig. 8 Time-averaged nondimensional harvested electrical power, η_2, as functions of reduced velocity

As expected, the results at n=2 reveal some aspects already observed in the nondimensional electric voltage. It can be noticed a slight enhancement in the values of $\bar{\eta}_2$ for reduced velocities lower than 5 when compared to the no parametric excitation case. At U_r=20 there is a jump in the plot, in agreement with the jump in v^{std} observed in Fig. 3. In the intermediate interval 5<U_r<20 the extracted power is significantly smaller than under no parametric excitation.

On the other hand, at n=1, the harvested electric power is larger than that in the pure galloping case within a wide range, 8<U_r<25, being significantly larger just after the jump at $U_r \approx 14$.

Notice that there are some ranges of reduced velocity in

which parametric excitation enhances the energy harvested from galloping. Hence, it is interesting to plot the variations of $\gamma_1(n)$ and $\gamma_2(n)$ - the ratios between harvested powers at n with respect to the pure galloping case - as defined in Eqs. (11) and (12), as functions of U_r.

Fig. 9 presents the variation of γ_1 with U_r. It is clearly noticeable that at reduced velocities lower than 9, the parametric excitation at n=2 enhances the power dissipated at the dashpot. Such an augment is close to 30% at U_r =3.2 and is associated to the higher oscillation frequency (see Fig. 6). Notice also that this result agrees with the previous findings herein obtained, indicating that the parametric instability at n=2 dominates the galloping response for low values of reduced velocity. Still considering this parametric excitation frequency, the power dissipated at the dashpot is lower than that obtained for the pure galloping case, for U_r>9.

On the other hand, at n=1 the power dissipated at the dashpot is enhanced by less than 10% in the range $14<U_r<30$.

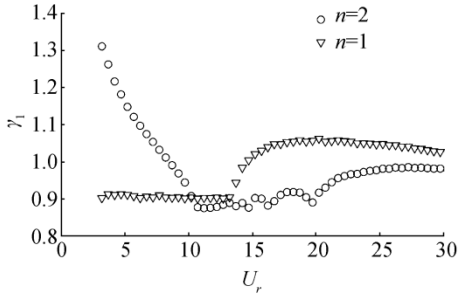

Fig. 9 Variation of γ_1, ratio of harvested power at the dashpot with respect to that of pure galloping case, as functions of the reduced velocity

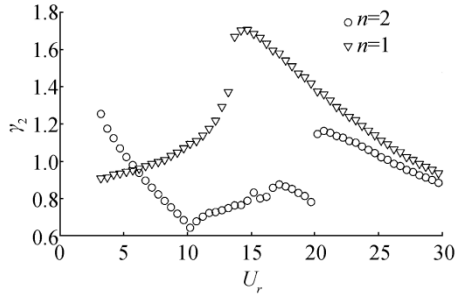

Fig. 10 Variation of γ_2, ratio of harvested electrical power with respect to that of pure galloping case, as functions of the reduced velocity

Finally, Fig. 10 shows the variation of γ_2 with the reduced velocity. At n=2, there are two ranges of reduced velocity in which the parametric excitation enhances the harvested electrical power, namely $3.2<U_r<5$ and $20<U_r<25$. In both intervals, the maximum enhancement is close to 20%. At n=1, Fig. 10 reveals an enhancement of the harvested electric power for $9<U_r<28$, with a significant maximum of 70% at $U_r \approx 14$.

Focus is now put on the variation of the prism oscillations and the harvested powers as continuous functions of n and δ. Such analysis is made considering a particular reduced velocity, namely U_r=14. This value corresponds to the peak of γ_2 – see Fig. 10.

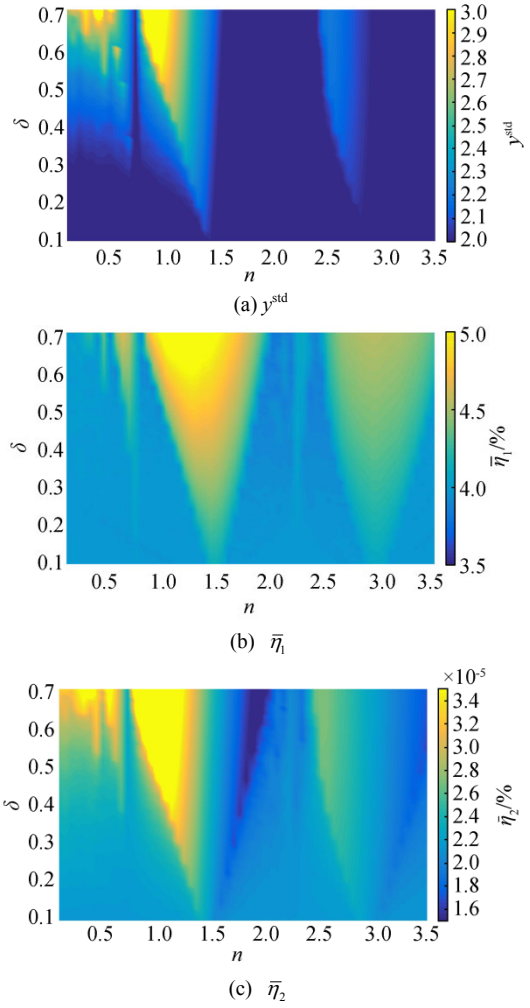

Fig. 11 Amplitude maps of y^{std}, $\bar{\eta}_1$ and $\bar{\eta}_2$ with n and δ; U_r=14

Fig. 11 presents a continuous color map for the variations of y^{std}, $\bar{\eta}_1$ and $\bar{\eta}_2$ with respect to amplitude and frequency of the parametric excitation. These plots reveal an interesting aspect. Contrary to what would be expected, the parametric excitation at n=2 (principal Mathieu instability) is not the case leading to the largest amplification in either, oscillations and harvested power. Notice that iso-surfaces arise from $n \approx 1.5$, different from what is observed in the transition curves of the Strutt diagrams for the linear Mathieu equation, at n=2. This non-intuitive result certainly needs a more detailed investigation from the analytical point-of-view. This is left for further work.Before addressing the conclusions, it is important to emphasize that the motivation of this paper lies on the fact that slender offshore structures are subjected to parametric excitation caused by the vertical motions of floating units associated to surface waves. In those cases, the source of parametric

excitation is the environmental condition and, hence, provided by nature.

A last aspect that should be pointed out is the character of the parametric excitation found in the offshore scenario. In this paper, focus is put on monochromatic sinusoidal time-varying stiffness. However, the motions of the floating units and, consequently, the geometric stiffness of slender structures attached to them, are multi-chromatic. In fact, multi-frequency parametric excitation is a very important matter in offshore engineering applications and should be studied further.

4 Conclusions

This paper addressed the piezoelectric energy harvesting from galloping phenomenon combined with parametric excitation. A reduced-order model was proposed in nondimensional form and numerically integrated in time. Particularly, two parametric excitation frequencies were studied, n=1 and n=2, being n the ratio between the excitation frequency and the natural frequency of the structure under no piezoelectric coupling.

It was found that the parametric excitation modifies both the structural oscillations and the electric voltage obtained at the load resistance. For reduced velocities higher than14, parametric excitation at n=1 increased both structural oscillations and electric voltage when compared to the pure galloping problem. For low values of reduced velocity, parametric excitation at n=2 leads to larger oscillations and electric voltage. This latter aspect indicates that the principal parametric instability (i.e., that obtained with n=2) dominates galloping for low reduced velocities.

Parametric excitation also affects the power dissipated at both the dashpot and the electric resistance. For low values of reduced velocity, parametric excitation at n=2 increases the harvested power when compared to the pure galloping case. On the other hand, parametric excitation at n=1 leads to a marked increase in the electrical harvested power. Particularly, there is a maximum enhancement of harvested electrical power, close to 70%, at n=1 and reduced velocity close to14.

A more extensive study regarding the influence of the different parameters that govern the dynamics of the electric-fluid-mechanic system on energy harvesting is under way. Further work may include a deeper investigation on the dynamics of a body subjected to concomitant galloping and parametric excitation, including Computational Fluid Dynamics simulations and experimental investigations. Analytical investigations on the equations of motion may also reveal interesting insights on the dynamics of the electro-fluid-mechanic system.

Acknowledgements

The first and the thrid authors acknowledge National Research Council – CNPq for grants 310595/2015-0 and 308990/2014-5. The second author acknowledges undergraduate scholarship provided by University of São Paulo research nucleous NAP-OS (Nucleous for Research Support – Sustainable Ocean).

Nomenclature

m_s	Structural mass
m_a	Added mass
D, L	Square side and prism length, respectively
$k(t)$, c	Stiffness and damping constant of the support
C_D	Drag coefficient
Y, V	Dimensional prism displacement and electrical voltage, respectively
Δk, Ω	Parametric excitation amplitude and frequency, respectively
C_p, R, θ	Capacitance, resistance and electromechanical coupling term of the piezoelectric circuit, respectively
t, τ	Time and its dimensionless form
$\boldsymbol{U}_\infty$	Free-stream velocity
P_D, P_{el}	Dimensional power dissipated at the dashpot and at the piezoelectric circuit
y, v	Dimensionless prism displacement and electrical voltage, respectively
m^*, C_a	Mass ratio parameter and added mass coefficient, respectively
ζ_s	Structural damping ratio
δ, n	Dimensionless amplitude and frequency ratio of the parametric excitation, respectively
a_1, a_2, a_3, σ_1	Dimensionless parameters of the mathematical model
η_1, η_2	Dimensionnless power dissipated at the dashpot and at the piezoelectric circuit, respectively

References

Barrero-Gil A, Alonso G, Sanz-Andres A, 2010. Energy harvesting from transverse galloping. *Journal of Sound and Vibration*, **329**, 2873-2883.
DOI: http://dx.doi.org/10.1016/j.jsv.2010.01.028

Bernitsas MM, Raghavan K, Ben-Simos Y, Garcia EMH, 2006a. VIVACE (Vortex Induced Vibration Aquatic Clean Energy): A new concept in generation of clean and renewable energy from fluid flow. *Proceedings of OMAE2006 - International Conference on Offshore Mechanics and Artic Engineering*, Hamburg.
DOI: 10.1115/OMAE2006-92645

Bernitsas MM, Ben-Simos Y, Raghavan K, Garcia EMH, 2006b. The VIVACE converter: model tests at high damping and Reynolds number around 10^5. *Proceedings of OMAE2006 - International Conference on Offshore Mechanics and Artic Engineering*, Hamburg.

Bibo A, Daqaq MF, 2013. Energy harvesting under combined aerodynamic and base excitations. *Journal of Sound and Vibration*, **332**, 5086-5102.
DOI: http://dx.doi.org/10.1016/j.jsv.2013.04.009

Blevins R, 2001. Flow-induced vibration. *Krieger.*

Doaré O, Michelin S, 2011. Piezoelectric coupling in energy

harvesting fluttering flexible plates: linear stability analysis and conversion efficiency. *Journal of Fluids and Structures*, **27**, 1357-1375.
DOI: http://dx.doi.org/10.1016/j.jfluidstructs.2011.04.008

Faltinsen OM, 1993. Sea loads on ships and offshore structures. *Dover Publications*.

Fernandes AC, Armandei M, 2014. Low-head hydropower extraction based on torsional galloping. *Renewable Energy*, **69**, 447-452.
DOI: http://dx.doi.org/10.1016/j.renene.2014.03.057

Franzini GR, Mazzilli CEN, 2016. Nonlinear reduced-order model for parametric excitation of vertical and immersed slender rod. *International Journal of Non-linear Mechanics*, **80**, 29-39.
DOI: http://dx.doi.org/10.1016/j.ijnonlinmec.2015.09.019

Franzini GR, Pesce CP, Salles R, Gonçalves RT, Fujarra ALC, Mendes P, 2015. Experimental investigation with a vertical and flexible cylinder in water: response to top motion excitation and parametric resonance. *Journal of Vibration and Acoustics*, **137**(3), 031010–1 – 031010–12.
DOI: http://dx.doi.org/10.1115/1.4029265

Franzini GR, Pesce CP, Gonçalves RT, Mendes P, 2016a. Experimental investigations on Vortex-Induced Vibrations with a long flexible cylinder. Part II: effect of axial motion excitation in a vertical configuration. *Proceedings of the 11th International Conference on Flow-Induced Vibration – FIV2016*, the Hague, the Netherlands.

Franzini GR, Santos RCS, Pesce CP, 2016b. Energy harvesting from transverse galloping enhanced by parametric excitation. *Proceedings of the 11th International Conference on Flow-Induced Vibration – FIV2016*, the Hague, the Netherlands.

Grouthier C, Michelin S, Bourguet R, Modarres-Sadeghi Y, De Langre E, 2014. On the efficiency of energy harvesting using vortex-induced vibrations of cables. *Journal of Fluids and Structures*, **49**, 427-440.
DOI: http://dx.doi.org/10.1016/j.jfluidstructs.2014.05.004

Grouthier C, Michelin S, De Langre E, 2012. Optimal energy harvesting by vortex-induced vibrations in cables. *Proceedings of the 10th FIV 2012 - International Conference on Flow-Induced Vibrations Conference (& Flow-Induced Noise)*, Dublin.

Hoerner SF, 1965. Fluid-dynamic drag. *Hoerner Fluid Dynamics.*

Korotkin AI, 2009. Added masses of ship structures. *Springer.*

Mehmood A, Abdelkefi A, Hajj AA, Nayfeh AH, Akthar I, Nuhait, AO, 2013. Piezoelectric energy harvesting from vortex-induced vibrations of circular cylinder. *Journal of Sound and Vibration*, **332**, 4656-4667.
DOI: http://dx.doi.org/10.1016/j.jsv.2013.03.033

Meirovitch L, 2003. Methods of analytical dynamics. *Dover Publications.*

Nayfeh AH, Mook DT, 1979. Nonlinear oscillations. *John Wiley & Sons.*

Païdoussis MP, Price SJ, De Langre E, 2011. Fluid-structure interactions - cross-flow induced instabilities. *Cambridge University Press*, Cambridge.

Patel MH, Park HI, 1991. Dynamics of tension leg platform tethers at low tension. Part I – Mathieu instability at large parameters. *Marine Structures*, **4**, 257-273.

Simos AN, Pesce CP, 1997. Mathieu stability in the dynamics of TLP's tethers considering variable tension along the length. *Transactions on the Built Environment*, **29**, 175-186.

Tang L, Païdoussis MP, Jiang J, 2009. Cantilever flexible plates in axial flow: Energy transfer and the concept of flutter-mill. *Journal of Sound and Vibration*, **326**, 263-276.
DOI: http://dx.doi.org/10.1016/j.jsv.2009.04.041

Xia Y, Michelin S, 2015. Fluid-solid-electric lock-in of energy harvesting piezoelectric flags. *Physical Review Applied*, **3**(014009), 014009–1–014009–8.
DOI: http://dx.doi.org/10.1103/PhysRevApplied.3.014009

Appendix

An investigation on the dependence of C_D

This appendix presents a discussion on the effects of the mean drag coefficient on the oscillations amplitude obtained under combined galloping and parametric excitation. Three values of drag coefficients were simulated, being one of them that used in the above simulations; one higher and another below this value.

Fig. A1 presents the standard-deviation of the prism displacements as a function of the reduced velocity for different drag coefficients considering parametric excitation at n=1. One clearly notices that there is no significant difference in the curves obtained for the three values of C_D. As expected, the larger the drag coefficient, the smaller the standard-deviation of the structural oscillations.

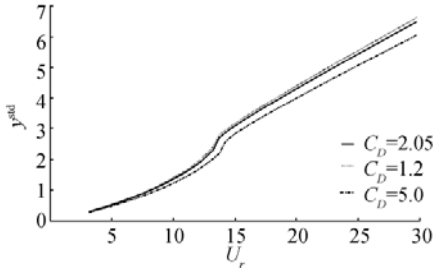

Fig. A1 Standard-deviation of $y(\tau)$ as functions of reduced velocity for different drag coefficients at n=1

The variation of y^{std} with the reduced velocity at n=2 is presented in Fig. A2. There is almost no difference between the results obtained with C_D=1.2 and 2.05. Close to U_r=20 at which the jump in the curve is observed, the differences between the case C_D=5.0 and the other values simulated are more pronounced.

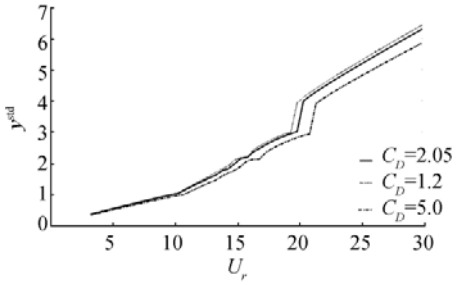

Fig. A2 Standard-deviation of $y(\tau)$ as functions of reduced velocity for different drag coefficients at n=2